Advances in Geo-Energy Research

Vol. 10, No. 1, p. 1-6, 2023

Short communication

Theoretical assessment of CO_2 injection into low-temperature water zones for non-leaking storage in hydrate form

Boyun Guo, Peng Zhang*

College of Engineering, University of Louisiana at Lafayette, Lafayette LA 70504, USA

Keywords:
CO_2 storage
frac-pack
well injectivity
permissible pressure
analytical model

Cited as:
Guo, B., Zhang, P. Theoretical assessment of CO_2 injection into low-temperature water zones for non-leaking storage in hydrate form. Advances in Geo-Energy Research, 2023, 10(1): 1-6.
https://doi.org/10.46690/ager.2023.10.01

Abstract:
Concerns exist about CO_2 leaks from conventional supercritical CO_2 storage reservoirs. This study investigates injecting CO_2 into low-temperature offshore reservoirs to lock it in a solid state, thus preventing potential leaks. An analytical model was developed to predict CO_2 injectivity into frac-packed injection wells in these low-temperature reservoirs. While the initial transient flow model was complex with Bessel functions and exponential integral, it was further simplified for practical field application. Sensitivity analysis of the model reveals that injectivity is less sensitive to reservoir permeability but more sensitive to fracture conductivity. The analytical model suggests injectivity is directly proportional to fracture width and fracture permeability. The case study utilizing field data from the South China Sea indicates feasible injection rates ranging from 6 to 17 tons/day depending on fracture conductivity. This work provides an analytical tool to predict injectivity for CO_2 storage in frac-packed low-temperature offshore reservoirs, contributing to carbon reduction and neutralization goals.

1. Introduction

The increasing level of CO_2 in the atmosphere is of great concern to humankind due to its global warming effect (Frölicher et al., 2014; Soeder, 2021). A number of carbon capture and storage projects have been initiated in recent years to place CO_2 in offshore structures like depleted oil reservoirs (Gaurina-Medimurec and Mavar, 2019; Sukor et al., 2020). Recent studies indicate a high risk of CO_2 leakage through CO_2-exposed oil wells (Hangx et al., 2016; Duguid et al., 2017). The leakage could be due to the loss of sealing integrity of wellbore cement over time from CO_2-cement interaction. Simulations by Zhang et al. (2021) show it may take centuries for CO_2 to fully penetrate wellbore cement through pore space to reach casing, but just months through cement cracks. Such cement cracks were presented in studies like Duguid et al. (2017). Since deterioration of wellbore cement sheath sealing is unavoidable, the high mobility of CO_2 in its supercritical state in offshore reservoirs is logically to "blame" (Lin et al., 2020; Anya et al., 2023). It is highly desirable to store CO_2 in its hydrate (solid-state) form in low-temperature offshore structures to minimize leakage.

By comparing the formation conditions of CO_2 hydrates and methane hydrates (Fig. 1), it is found that environments suitable for methane hydrate formation are also likely to provide conditions conducive to storing CO_2 in hydrate form. Since methane-hydrate reservoirs have been found globally in both onshore and offshore sediments (Kvenvolden, 1993; Dawe et al., 2007; Shaibu et al., 2021), it is logical to believe the number of low-temperature offshore structures is at least as many as the number of methane-hydrate reservoirs. Therefore, the potential for safely storing CO_2 in low-temperature offshore structures is huge.

Injecting CO_2 into methane-hydrate reservoirs for storage, called CH_4-CO_2 swapping, has been studied for years. In this process, one CO_2 molecule replaces one CH_4 molecule without destroying the hydrate structure or producing much water. This reduces matrix collapse and stratum failure (Cha et al., 2023). However, swapping efficiency is low due to mass transfer barriers caused by CO_2-hydrate formation (Davies et

Yandy Scientific Press

*Corresponding author.
E-mail address: boyunguo@163.com (B. Guo); peng.zhang1@louisiana.edu (P. Zhang).

Received August 15, 2023; revised August 26, 2023; accepted September 5, 2023; available online September 8, 2023.

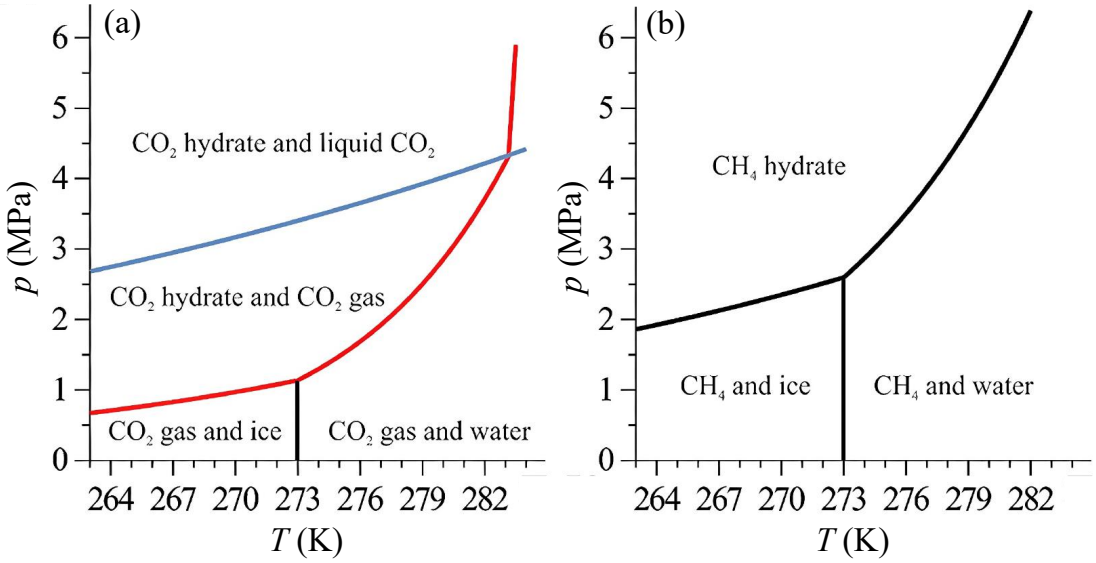

Fig. 1. Phase equilibrium curves for CO_2 and CH_4 (Khasanov et al., 2020): (a) CO_2, (b) CH_4.

al., 2010).

This study investigates storing CO_2 in low-temperature, low-permeability formations beneath the seafloor, assuming the CO_2 stream is heated prior to injection to prevent hydrate formation during injection. Injecting CO_2 into these formations at commercial rates is challenging due to the extremely low well injectivity. This investigation put forth frac-packing technology, commonly utilized to control sand production (Ghalambor et al., 2009), as a means to complete CO_2 injection wells and improve injectivity (Fig. 2). Although it remains uncertain whether frac-packed wells will attain adequate CO_2 injectivity, fracture orientation and dimensions are believed to play a pivotal role in determining the injectivity of fractured wells. Since vertical stress is the minimum in shallow formations below the seafloor, horizontal fractures are expected to propagate during frac-packing operations in these low-temperature formations (Lamont and Jessen, 1963; Huang et al., 2012; Lu et al., 2015). In this work, a mathematical model was formulated to predict CO_2 injectivity into frac-packed reservoirs with horizontal fractures. Sensitivity analysis shows CO_2 injectivity is less sensitive to reservoir permeability but more sensitive to fracture properties like width and permeability. Additionally, CO_2 injectivity is proportional to fracture permeability and width.

2. Mathematical model

2.1 Assumptions

The following assumptions are made to derive the governing equation for fluid injection into storage reservoirs through radial fractures:

1) The fluid storage reservoir is homogeneous and isotropic within boundaries.
2) The reservoir is fully saturated with a slightly compressible liquid.
3) Fluid is injected through a radial fracture at the mid-depth of the storage reservoir section.
4) The width of the radial fracture is constant.
5) Vertical flow of injected CO_2 dominates fluid seepage in the storage reservoir sections above and below the horizontal fracture.
6) Vertical flow of injected CO_2 supports the diverging radial flow in the fracture.

2.2 Governing equation

Consider a volume element of fracture at a radial distance r from the wellbore centerline, with a width in the tangential direction $r\mathrm{d}\theta$, a length in the radial direction $\mathrm{d}r$, and a height w (Fig. 2). The law of conservation of mass states:

Mass inflow rate − Mass outflow rate = Mass change rate in the volume element.

That is:

$$q\rho|_r - q\rho|_{r+\mathrm{d}r} - Q_m = \varphi_f w r \mathrm{d}r \mathrm{d}\theta \frac{\partial \rho}{\partial t} \tag{1}$$

where q is the fluid injection rate, ρ is the fluid density, φ_f is fracture porosity, t is the injection time, and Q_m is the mass flow rate from the fracture element into the matrix. All variables in this paper are in Darcy units. This equation can be expanded as:

$$q\rho|_r - \left[q\rho|_r + \frac{\partial(q\rho)}{\partial r}\mathrm{d}r\right] - Q_m = \varphi_f w r \mathrm{d}r \mathrm{d}\theta \frac{\partial \rho}{\partial t} \tag{2}$$

which is simplified to:

$$\frac{\partial(q\rho)}{\partial r}\mathrm{d}r + Q_m = -\varphi_f w r \mathrm{d}r \mathrm{d}\theta \frac{\partial \rho}{\partial t} \tag{3}$$

Applying Darcy's law gives:

$$q = -\frac{k_f w r \mathrm{d}\theta}{\mu}\frac{\partial p_f}{\partial r} \tag{4}$$

where k_f is the permeability of fracture, p_f is the pressure in the fracture at distance r, μ is fluid viscosity. The fluid volume V on one side of the fracture can be determined as:

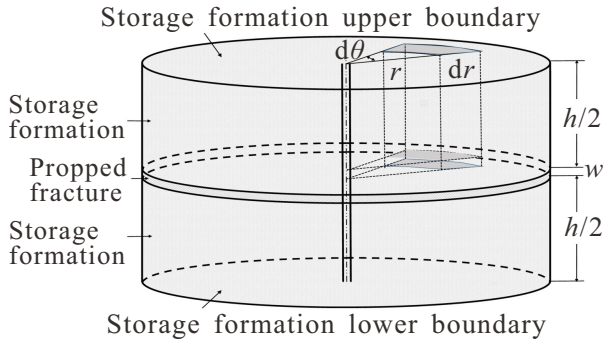

Fig. 2. A frac-packed storage reservoir separated by a horizontal radial fracture at the mid-depth.

$$V = \varphi \frac{h}{2} r \mathrm{d}\theta \mathrm{d}r \tag{5}$$

where φ is the matrix porosity, and h is the reservoir thickness.

The compression coefficient of matrix c_m is:

$$c_m = -\frac{1}{V}\frac{\partial V}{\partial p} \tag{6}$$

where p is pressure in matrix.

Differentiation of Eq. (5) with respect to time gives:

$$c_m V \frac{\partial \rho}{\partial t} = -\frac{\partial V}{\partial t} = -Q(r) \tag{7}$$

where $Q(r)$ is the mass flow rate at r.

Considering Eq. (5), the pressure increase rate $\partial p/\partial t$ in Eq. (7) can be solved to give:

$$\frac{\partial p}{\partial t} = -\frac{Q(r)}{c_m V} = -\frac{2Q(r)}{c_m \varphi h r \mathrm{d}\theta \mathrm{d}r} \tag{8}$$

The governing equation for the linear flow from the fracture element to the storage reservoir element is (Dake, 1983):

$$\frac{\partial^2 p}{\partial y^2} = \frac{\varphi \mu c_m}{k_m}\frac{\partial \rho}{\partial t} \tag{9}$$

where y is the depth of a location in a storage reservoir, k_m is reservoir permeability.

Substituting Eq. (8) into Eq. (9) gives:

$$\frac{\partial^2 p}{\partial y^2} = -\frac{2\mu Q(r)}{k_m h r \mathrm{d}\theta \mathrm{d}r} \tag{10}$$

Integrating Eq. (10) gives:

$$\frac{\partial p}{\partial y} = -\frac{2\mu Q(r)}{k_m h r \mathrm{d}\theta \mathrm{d}r} y + C_1 \tag{11}$$

where the integration constant C_1 can be evaluated by applying the boundary condition:

$$\left(\frac{\partial p}{\partial y}\right)_{y=h/2} = 0 \tag{12}$$

Applying Eq. (12) to (11) yields:

$$C_1 = \frac{2\mu Q(r)}{k_m r \mathrm{d}\theta \mathrm{d}r} \tag{13}$$

Substituting Eq. (13) into Eq. (11) gives:

$$\frac{\partial p}{\partial y} = \frac{2\mu Q(r)}{k_m r \mathrm{d}\theta \mathrm{d}r}\left(\frac{1}{2} - \frac{y}{h}\right) \tag{14}$$

Separating variables and integrating Eq. (14) results in:

$$p = \frac{2\mu Q(r)}{k_m r \mathrm{d}\theta \mathrm{d}r}\left(\frac{y}{2} - \frac{y^2}{2h}\right) + C_2 \tag{15}$$

where the integration constant C_2 can be calculated by applying the boundary condition:

$$p|_{y=0} = p_f \tag{16}$$

Applying Eq. (16) to Eq. (15) yields:

$$C_2 = p_f \tag{17}$$

Substituting Eq. (17) into Eq. (15) gives:

$$p = \frac{2\mu Q(r)}{k_m r \mathrm{d}\theta \mathrm{d}r}\left(\frac{y}{2} - \frac{y^2}{2h}\right) + p_f \tag{18}$$

Because along the boundary at $y = h/2$ the pressure is p_e (reservoir pressure), Eq. (18) yields:

$$Q(r) = \frac{4k_m r \mathrm{d}\theta \mathrm{d}r}{\mu h}\left(p_f - p_e\right) \tag{19}$$

The total mass flow rate to the storage reservoir matrix elements on both sides of the fracture is written as:

$$Q_m = 2\rho Q(r) = \frac{8\rho k_m r \mathrm{d}\theta \mathrm{d}r}{\mu h}\left(p_f - p_e\right) \tag{20}$$

The change of density in Eq. (3) can be formulated in terms of pressure change by incorporating the compressibility of the fluid:

$$\frac{\partial \rho}{\partial t} = c_f \rho \frac{\partial p_f}{\partial t} \tag{21}$$

where c_f is fluid compressibility in the fracture. Substituting Eqs. (4), (20), and (21) into Eq. (3) result in a governing equation for fluid flow inside the fracture element:

$$\frac{1}{r}\frac{\partial}{\partial r}\left(-r\frac{\partial p_f}{\partial r}\right) + \frac{8k_m}{hk_f w}\left(p_f - p_e\right) = -\frac{\varphi_f \mu c_f}{k_f}\frac{\partial p_f}{\partial t} \tag{22}$$

Define a pressure differential p_d as:

$$p_d = p_f - p_e \tag{23}$$

Substituting Eq. (23) into Eq. (22) gives:

$$\frac{1}{r}\frac{\partial}{\partial r}\left(r\frac{\partial p_d}{\partial r}\right) = \frac{\varphi_f \mu c_f}{k_f}\frac{\partial p_d}{\partial t} + \frac{8k_m}{hk_f w}p_d \tag{24}$$

If the coefficient groups $\varphi_f \mu c_f / k_f$ and $8k_m/hk_f w$ are denoted by A and B, respectively, Eq. (24) can be simplified to give:

$$\frac{1}{r}\frac{\partial}{\partial r}\left(r\frac{\partial p_d}{\partial r}\right) = A\frac{\partial p_d}{\partial t} + Bp_d \tag{25}$$

2.3 Initial and boundary conditions

The initial condition is that pressure remains constant everywhere before the fluid injection is activated:

$$p_d = 0 \text{ at } t = 0, \text{ for all } r \tag{26}$$

For the outer boundary far away from the wellbore is specified by:

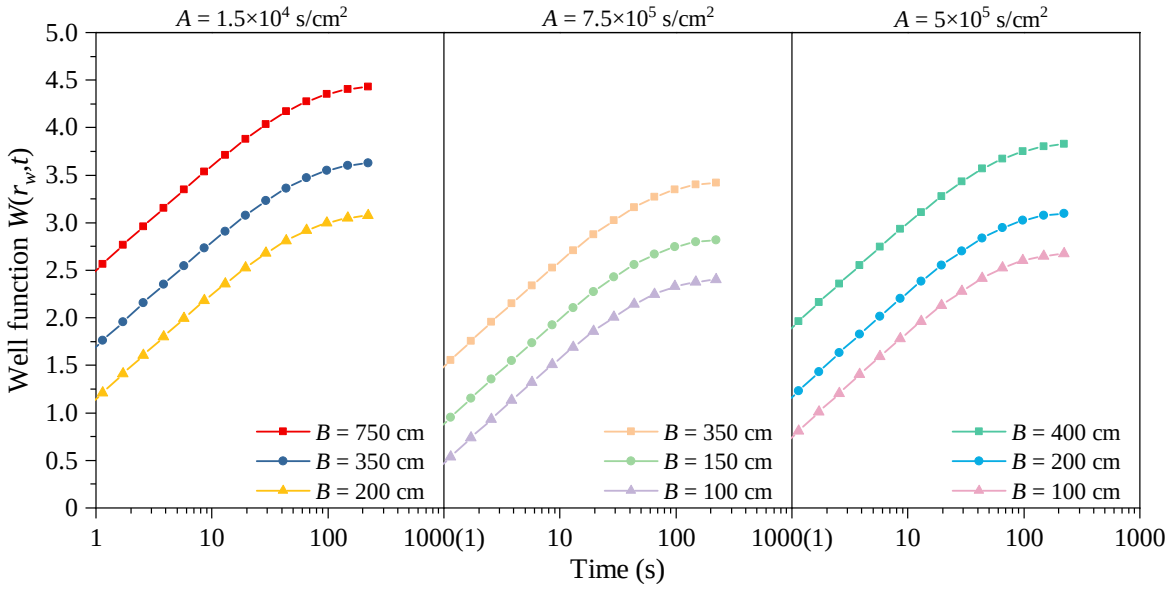

Fig. 3. Plots of $W(r_w,t)$ for practical A, and B values.

$$p_d = 0 \text{ at } r = \infty, \text{ for all } t \tag{27}$$

For the inner boundary, it holds:

$$\lim_{r\to 0}\left(r\frac{\partial p_d}{\partial r}\right) \equiv \frac{q\mu}{2\pi w k_f}, \text{ for } t > 0 \tag{28}$$

2.4 Solution

The solution of Eq. (25) with the initial and boundary conditions is:

$$\begin{aligned} p_d = \frac{q\mu}{2\pi w k_f}\Bigg\{ & K_0\left(\frac{r}{B}\right) - \frac{1}{2} I_0\left(\frac{r}{B}\right) Ei\left(\frac{t}{AB^2}\right) \\ & + \frac{1}{2}\exp\left(-\frac{t}{AB^2}\right)\left[\ln\left(\frac{\gamma A r^2}{4t}\right) + Ei\left(\frac{Ar^2}{4t}\right)\right. \\ & \left. -\frac{Ar^2}{4t} + \frac{Ar^2}{4t}\frac{I_0\left(\frac{r}{B}\right)-1}{\left(\frac{r}{2B}\right)^2}\right]\Bigg\} \end{aligned} \tag{29}$$

where I_0 is the zero-order modified Bessel function of the first kind, K_0 is the zero-order modified Bessel function of the second kind, Ei is the exponential integral, and γ is an exponential function of Euler's constant ($e^{0.5572} = 1.75$).

Eq. (29) simplifies to the expression for the pressure differential in the wellbore where $r = r_w$ (i.e., wellbore radius):

$$p_d = \frac{q\mu}{2\pi w k_f} W(r_w,t) \tag{30}$$

where the well function $W(r_w,t)$ is given by:

$$\begin{aligned} W(r_w,t) = {} & K_0\left(\frac{r_w}{B}\right) - \frac{1}{2} I_0\left(\frac{r_w}{B}\right) Ei\left(\frac{t}{AB^2}\right) \\ & + \left[\ln\left(\frac{\gamma A r_w^2}{4t}\right) + Ei\left(\frac{Ar_w^2}{4t}\right) - \frac{Ar_w^2}{4t} + \frac{Ar_w^2}{4t}\frac{I_0\left(\frac{r_w}{B}\right)-1}{\left(\frac{r_w}{2B}\right)^2}\right] \\ & * \frac{1}{2}\exp\left(-\frac{t}{AB^2}\right) \end{aligned} \tag{31}$$

To rearrange Eq. (30), q is described by the following equation:

$$q = \frac{2\pi w k_f (p_w - p_e)}{\mu W(r_w,t)} \tag{32}$$

where p_w is the wellbore pressure.The mathematical model is challenging to use since the functions are difficult to evaluate, which necessitates model simplification for practical applications. Fig. 3 presents well function $W(r_w,t)$ curves for practical A and B values. The curves all level off after an injection time of around 100 seconds. This means the time-dependent terms in $W(r_w,t)$ diminish after a short injection period which is negligible in real applications. After removing the time-dependent terms the well function can be simplified to:

$$W(r_w,t) = K_0\left(\frac{r_w}{B}\right) \tag{33}$$

For practical values of r_w and B, the ratio r_w/B is close to zero. Because $\lim_{x\to 0} K_0(x) \equiv \ln(2/\gamma x)$, the relation $\lim_{(r_w/B)\to 0} K_0(r_w/B) \equiv \ln(2B/\gamma r_w)$ holds. Therefore, Eq. (33) practically degenerates to:

$$W(r_w,t) = \ln\left(\frac{2B}{\gamma r_w}\right) \tag{34}$$

Submitting coefficient group B, and Eq. (34) into Eq. (32) yields a simplified form of solution:

$$q = \frac{2\pi w k_f (p_w - p_e)}{\mu \ln\left(\frac{2}{\gamma r_w}\sqrt{\frac{hk_f w}{8k_m}}\right)} \tag{35}$$

The maximum permissible fluid injection rate is the injection rate when the wellbore pressure (pressure at the entry of fracture) reaches the minimum in-situ stress $s_{\min}$ when the overburden is lifted.

Submitting $p_w = s_{\min}$ into Eq. (35) results in:

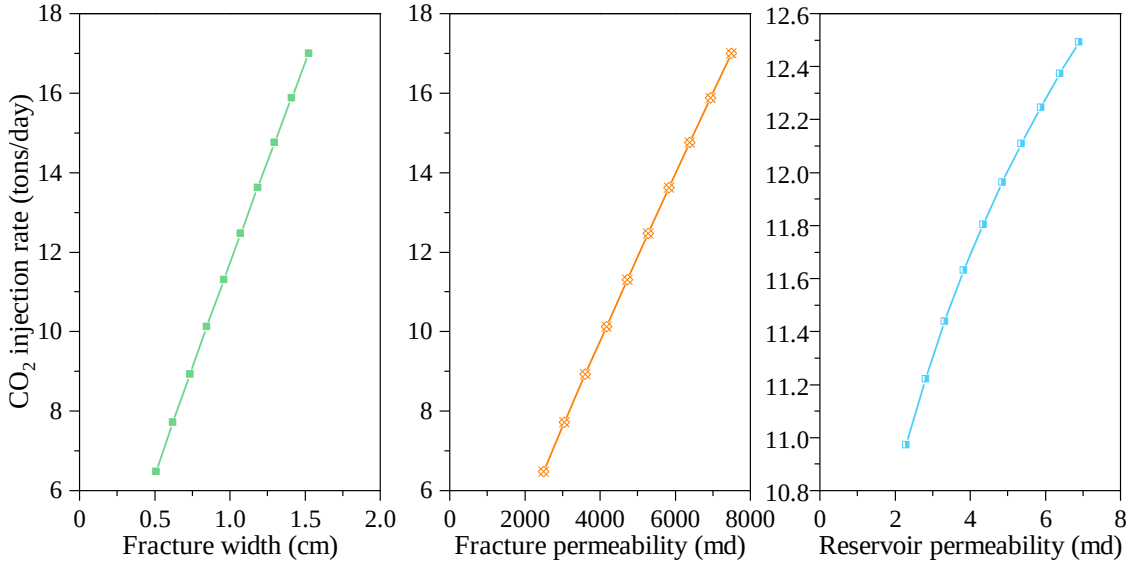

Fig. 4. Effects of fracture width, fracture permeability, and reservoir permeability on CO_2 injectivity.

$$q_{\max} = \frac{2\pi w k_f (s_{\min} - p_e)}{\mu \ln\left(\frac{2}{\gamma r_w}\sqrt{\frac{h k_f w}{8 k_m}}\right)} \tag{36}$$

It is understood that the volumetric flow rate $q_{\max}$ is in reservoir condition. If the density of the fluid is known at the reservoir pressure and temperature, the maximum permissible fluid mass injection rate can be calculated.

3. Sensitivity analysis

Eq. (36) implies the maximum permissible fluid injection rate is directly proportional to the differential between vertical stress and initial reservoir pressure, known as the effective vertical stress, which is typically well characterized. Reservoir thickness is also usually known confidently. The equation also shows the maximum injection rate is inversely proportional to fluid viscosity, which is logically understandable from a frictional pressure perspective. However, data on reservoir permeability, fracture width, and fracture permeability are usually uncertain. Due to uncertainty in these parameter values, conducting sensitivity analysis would be prudent to identify factors significantly impacting the injection rate.

The storage reservoir condition is similar to that found in a low-temperature reservoir below the sea floor (Liu et al., 2012). The data set used in the sensitivity analysis is listed in Table 1. The model-calculated effects of reservoir permeability, fracture width, and fracture permeability on CO_2 injectivity are seen in Fig. 4. It reveals that injectivity varies nonlinearly with reservoir permeability changes, indicating relatively low sensitivity. However, injectivity varies linearly with changes in fracture width and fracture permeability, showing high sensitivity. Though reservoir permeability changes by 50%, injectivity only varies about 5%-8% around the 11.9 tons/day mean. But with 50% changes in fracture width or permeability, injectivity varies by 42%. Therefore, fracture conductivity dominates injectivity, while reservoir permeability has a relatively minor effect.

Table 1. Reservoir and fracture properties for a subsea storage reservoir.

Parameter	Value
Water depth (cm)	100,613
Reservoir mid-depth (cm)	134,604
Reservoir temperature (°C)	6
Reservoir pressure (atm)	140
Minimum in-situ stress (atm)	181
Reservoir thickness (cm)	2,378
Reservoir permeability (Darcy)	0.0046
Fluid viscosity (cp)	0.8
Wellbore radius (cm)	10
Fracture width (cm)	1
Fracture permeability (Darcy)	5

4. Conclusions

This study proposes injecting CO_2 into subsea reservoirs with temperatures below CO_2-hydrate formation levels, enabling solid-state storage to minimize potential leakage. Assuming pre-injection CO_2 heating prevents reservoir hydrate formation, a mathematical solution was developed to predict injectivity into frac-packed reservoirs. Sensitivity analysis allows the following conclusions:

1) The developed transient model could be utilized to predict CO_2 injectivity, which was simplified to steady-state without early time dependencies for practical use.
2) Injectivity is less sensitive to reservoir permeability but more sensitive to fracture width and permeability. Increasing fracture conductivity, the product of width and permeability significantly improves injectivity.

3) The case study using data from a low-temperature reservoir shows achievable commercial injection rates of 6-17 tons/day depending on fracture conductivity.

These conclusions assume pore spaces remain fully occupied by supercritical CO_2 during injection, with flow velocities high enough to prevent hydrate formation. Solid-state CO_2 storage in appropriately frac-packed subsea reservoirs can therefore enable commercial-scale injection while minimizing leakage risks.

Acknowledgements

The authors are grateful to BIRD for funding the project "Safe, sustainable, and resilient development of offshore reservoirs and natural gas upgrading through innovative science and technology: Gulf of Mexico-Mediterranean," through Contract No. EC-19 Fossil Energy.

Conflict of interest

The authors declare no competing interest.

References

Anya, A., Emadi, H., Watson, M. A novel apparatus and method for lab-scale study of wellbore integrity using CT imaging and analysis. Journal of Petroleum Science and Engineering, 2023, 220: 111209.

Cha, M., Shin, K., Lee, H., et al. Kinetics of methane hydrate replacement with carbon dioxide and nitrogen gas mixture using in situ NMR spectroscopy. Environmental Science & Technology, 2015, 49(3): 1964-1971.

Dake, L. P. Fundamentals of Reservoir Engineering. New York, USA, Elsevier Science, 1983.

Davies, S. R., Sloan, E. D., Sum, A. K., et al. In situ studies of the mass transfer mechanism across a methane hydrate film using high-resolution confocal Raman spectroscopy. The Journal of Physical Chemistry C, 2010, 114(2): 1173-1180.

Dawe, R. A., Thomas, S. A large potential methane source-natural gas hydrates. Energy Sources, Part A, 2007, 29(3): 217-229.

Duguid, A., Guo, B., Nygaard, R. Well integrity assessment of monitoring wells at an active CO_2-EOR flood. Energy Procedia, 2017, 114: 5118-5138.

Frölicher, T. L., Winton, M., Sarmiento, J. L. Continued global warming after CO_2 emissions stoppage. Nature Climate Change, 2014, 4(1): 40-44.

Gaurina-Medimurec, N., Mavar, K. N. Carbon capture and storage (CCS): Geological sequestration of CO_2, in CO_2 Sequestration, edited by L. A. Frazao, A. M. Silva-Olaya, J. C. Silva, IntechOpen, London, pp. 1-21, 2019.

Ghalambor, A., Ali, S. A., Norman, W. D. Frac Packing Handbook. Richardson, USA, Society of Petroleum Engineers, 2009.

Hangx, S. J. T., Linden, A., Marcelis, F., et al. Defining the brittle failure envelopes of individual reaction zones observed in CO_2-exposed wellbore cement. Environmental Science & Technology, 2016, 50(2): 1031-1038.

Huang, J., Griffiths, D. V., Wong, S. W. Initiation pressure, location and orientation of hydraulic fracture. International Journal of Rock Mechanics and Mining Sciences, 2012, 49: 59-67.

Khasanov, M. K., Musakaev, N. G., Stolpovsky, M. V., et al. Mathematical model of decomposition of methane hydrate during the injection of liquid carbon dioxide into a reservoir saturated with methane and its hydrate. Mathematics, 2020, 8(9): 1482.

Kvenvolden, K. A. Gas hydrates-geological perspective and global change. Reviews of Geophysics, 1993, 31(2): 173-187.

Lamont, N., Jessen, F. W. The effects of existing fractures in rocks on the extension of hydraulic fractures. Journal of Petroleum Technology, 1963, 15(2): 203-209.

Lin, Y., Deng, K., Yi, H., et al. Integrity tests of cement sheath for shale gas wells under strong alternating thermal loads. Natural Gas Industry B, 2020, 7(6): 671-679.

Liu, C., Ye, Y., Meng, Q., et al. The characteristics of gas hydrates recovered from Shenhu Area in the South China Sea. Marine Geology, 2012, 307: 22-27.

Lu, C., Li, M., Guo, J. C., et al. Engineering geological characteristics and the hydraulic fracture propagation mechanism of the sand-shale interbedded formation in the Xu5 reservoir. Journal of Geophysics and Engineering, 2015, 12(3): 321-339.

Shaibu, R., Sambo, C., Guo, B., et al. An assessment of methane gas production from natural gas hydrates: Challenges, technology and market outlook. Advances in Geo-Energy Research. 2021, 5(3):318-32.

Soeder, D. J. Greenhouse gas sources and mitigation strategies from a geosciences perspective. Advances in Geo-Energy Research, 2021, 5(3): 274-285.

Sukor, N. R., Shamsuddin, A. H., Mahlia, T. M., et al. Techno-economic analysis of CO_2 capture technologies in offshore natural gas field: Implications to carbon capture and storage in Malaysia. Processes, 2020, 8(3): 350.

Zhang, P., Guo, B., Liu, N. Numerical simulation of CO_2 migration into cement sheath of oil/gas wells. Journal of Natural Gas Science and Engineering, 2021, 94: 104085.